# The Coherence Length Dependence on Doping of Cuprates

Shir Dobenco

# The Coherence Length Dependence on Doping of Cuprates

**Research Thesis**

**In Partial Fulfillment of The Requirements for the Degree of Master of Science in Physics**

**Shir Dobenco**

**Submitted to the Senate of the Technion - Israel Institute of Technology**

Adar, 5783, Haifa, March, 2023

The Research Thesis was done under the supervision of Professor Amit Keren in the Department of Physics.

The generous financial help of the Technion is gratefully acknowledged

The author of this thesis states that the research, including the collection, processing and presentation of data, addressing and comparing to previous research, etc., was done entirely in an honest way, as expected from scientific research that is conducted according to the ethical standards of the academic world. Also, reporting the research and its results in this thesis was done in an honest and complete manner, according to the same standards.

# Contents

# List of Figures

# Abstract

The superconducting stiffness $\hat{\rho}_s$ is the relation between the vector potential $\boldsymbol{A}$ and the current density $\boldsymbol{J}_s$ inside superconducting (SC) materials as described by the London equation $\boldsymbol{J}_s = -\hat{\rho}_s \boldsymbol{A}$. The coherence length $\xi$ is a measure of how large can $\boldsymbol{J}_s$ be.

We measure the superconducting stiffness and coherence length using the Stiffnessometer technique, developed in our group [1][2]. The measurement is done by the application of current in a thin and long excitation coil that pierces a SC ring-shaped sample, creating a rotor-free vector potential $\boldsymbol{A}$ inside the sample. According to London's equation, SC currents emerge, leading to a magnetic moment, which is measured using a superconducting quantum interference device (SQUID). This method does not suffer from demagnetization factors or the presence of vortices.

In this work, we measured the stiffness and coherence length of a $Bi_2Sr_2CaCu_2O_{8+x}$ (Bi-2212) sample with critical temperature of about $70K$, for different doping levels in the over-doped regime, with the same sample being oxidized following each measurement. Bi-2212 is a member of the cuprates, a family of High Temperature SC.

The results show the dependence of the stiffness and the coherence length on the doping level. Particularly, decreasing coherence lengths with increasing doping levels.

# Symbols and Abbreviations

## Abbreviations

Bi-2212 $Bi_2Sr_2CaCuO_{8+x}$

CP Cupper-Pair

GL Ginsburg Landau

HTSC High Temperature Super Conductors

PDE Partial Differential Equation

SC Superconductivity

SQUID Superconducting Quantum Interference Device

VSM Vibrate Sample Magnetometer

ZGFC Zero Gauge-Field Cooling

## Symbols

$\boldsymbol{A}$ Vector Potential

$A^c$ Critical Vector Potential

$B$ Total Magnetic Field

$c$ Speed of Light

$e$ Electron Charge

| | |
|---|---|
| $H$ | External Magnetic Field |
| $H_{c1}$ | First Superconducting Critical Field |
| $H_{c2}$ | Second Superconducting Critical Field |
| $I$ | Current |
| $\boldsymbol{J}_s$ | Current Density |
| $J_c$ | Critical current Density |
| $m$ | Magnetic Moment |
| $m_e$ | Electron Mass |
| $n$ | Windind Density of the Excitation Coil |
| $\hat{\varphi}$ | Azimuthal Direction |
| $\Phi$ | Magnetic Flux |
| $\varphi$ | Phase of the Complex Order Parameter |
| $\Phi_0$ | Flux Quanta |
| $\psi$ | Complex Order Parameter |
| $\rho$ | Resistivity |
| $\hat{\rho}_s$ | Superconducting Stiffness |
| $T$ | Temperature |

| | |
|---|---|
| $T_c$ | Critical Temperature |
| $T_N$ | Néel Temperature |
| $\boldsymbol{v}_c$ | Critical Velocity |
| $\xi$ | Coherence Length |

# 1 Introduction

## 1.1 Superconductivity

Superconductivity (SC) is a material phase characterized by unique phenomena such as zero resistance and perfect diamagnetism (Meissner Effect). Metalic SC can be explained using the BCS Theory [3] (named after John Bardeen, Leon Cooper and John Robert Schrieffer, introduced in 1957) which considers an attractive interaction between electrons through electron-phonon coupling. It is common to think of the charge carriers of a SC as pairs of electrons called Cooper-Pairs (CP) rather than individual electrons. The critical temperature $T_c$ refers to the characteristic temperature of the transition between the SC phase and the normal phase, where the material become a normal conductor with finite resistivity. The BCS theory predicts an upper limit for $T_c$; this upper limit is set by the cut-off freuency [4], and was believed to be $30K$, due to the conventional limitation on the phonon frequency at the time.

The coherence length $\xi$ is the size of the CP. $\xi$ is also the shortest length scale over which the phase of the complex order parameter (discussed in Sec 1.3) can vary. When applying a magnetic field to a SC, it will reject it by creating super-currents which screen the external magnetic field. If we increase the external field, the super-currents will also increase. But, although the field is expelled from the bulk, it penetrates along the edges with exponential decay and some characteristic length, known as the penetration

depth $\lambda$.

The SC materials can be divided into two types, depending on the ratio of $\xi$ and $\lambda$: a type-I SC have $\lambda < \xi/\sqrt{2}$ and a type-II SC have $\lambda > \xi/\sqrt{2}$ . A type-I SC will hold the magnetic field outside the bulk until we reach the critical field $H_c$, as above $H_c$ the material gives-up and transforms back to the normal state, letting all the magnetic flux go through it. A type-II SC will stay field-free up to some critical field $H_{c1}$, where above it, it is capable of letting some of the magnetic flux get in as vortices. The core of these vortices will maintain the normal state phase, and outside of the vortex the material will remain a SC. When we increase the external field, more vortices will get inside until they cover the entire material and all of it becomes normal at a second critical field $H_{c2}$.

In 1986, the $T_c$ limitation has been surpassed for the first time and a new family of high temperature SC materials was discovered: the Cuprates [5]. Those materials are defined by having a nearly tetragonal unit cell which forms layers of copper-oxide planes ($CuO_2$). This SC group will be discussed more in Sec 1.4.

## 1.2 The London Equation and the Meissner Effect

The superconducting stiffness $\hat{\rho}_s$ is defined by a local relation between the superconducting current density $\boldsymbol{J}_s$ to the vector potential $\boldsymbol{A}$ and the gradient of $\varphi$, the phase of the complex order parameter $\psi = |\psi|e^{i\varphi}$ (comes from

Landau's theory Sec 1.3) . This relation is:

$$\boldsymbol{J}_s = \hat{\rho}_s(\frac{\hbar c}{q}\boldsymbol{\nabla}\varphi - \boldsymbol{A}). \tag{1.1}$$

where $c$ is the speed of light and $q$ is the charge of the charge carriers. $\hat{\rho}_s$ is a diagonal tensor or an even scalar. This equation is gauge invariant. As we explain in Sec 2 in our experiments $\nabla\varphi = 0$ and we get:

$$\boldsymbol{J}_s = -\hat{\rho}_s\boldsymbol{A}. \tag{1.2}$$

If we use the rotor of Maxwell's equation: $\boldsymbol{\nabla}\times\boldsymbol{\nabla}\times\boldsymbol{B} = \frac{4\pi}{c}\boldsymbol{\nabla}\times\boldsymbol{J}$ (where $\boldsymbol{J}$ is the sum of normal and super currents) and the definition of $\boldsymbol{A}$: $\boldsymbol{B} = \boldsymbol{\nabla}\times\boldsymbol{A}$, we get a partial differential equation for the magnetic field $\boldsymbol{B}$:

$$\boldsymbol{\nabla}^2\boldsymbol{B} = \frac{4\pi}{c}\hat{\rho}_s\boldsymbol{B} \tag{1.3}$$

The solution (in one dimension) will be: $B = B_0 e^{-\frac{x}{\lambda}}$. This exponential decay of the magnetic field inside the bulk of a SC is called the Meissner Effect and it gives us the relation between the SC stiffness and the penetration depth $\lambda$:

$$\rho_s = \frac{c}{4\pi}\frac{1}{\lambda^2}. \tag{1.4}$$

## 1.3 The Ginzburg-Landau Approach

Another way to look at the superconducting phenomena is from the Ginzburg-Landau (GL) point of view (following [6]). Denoting the complex SC quantum state as $\psi = |\psi|e^{i\varphi}$ where $|\psi|^2$ is the density of the CP and $\varphi$ is the phase, the GL functional of the free energy is:

$$f = f_{n0} + \alpha|\psi|^2 + \frac{\beta}{2}|\psi|^4 + \frac{1}{2m^*}|(\frac{\hbar}{i}\boldsymbol{\nabla} - \frac{e^*}{c}\boldsymbol{A})\psi|^2 + \frac{(\nabla \times \boldsymbol{A})^2}{8\pi}. \tag{1.5}$$

To minimizes the free energy, we differentiate by $\psi^*$ and it gives:

$$\alpha\psi + \beta|\psi|^2\psi + \frac{1}{2m^*}(\frac{\hbar}{i}\boldsymbol{\nabla} - \frac{e^*}{c}\boldsymbol{A})^2\psi = 0 \tag{1.6}$$

minimizing with respect to $\boldsymbol{A}$ leads to:

$$\begin{aligned} \boldsymbol{J} &= \frac{c}{4\pi}\boldsymbol{\nabla} \times \boldsymbol{\nabla} \times \boldsymbol{A} \\ &= \frac{e^*\hbar}{2m^*i}(\psi^*\nabla\psi - \psi\nabla\psi^*) - \frac{e^{*2}}{m^*c}\psi^*\psi\boldsymbol{A} \\ &= \frac{e^*}{m^*}|\psi|^2(\hbar\boldsymbol{\nabla}\varphi - \frac{e^*}{c}\boldsymbol{A}) = e^*|\psi|^2\boldsymbol{v}_s \end{aligned} \tag{1.7}$$

where $\boldsymbol{v}_s$, $m^*$, $e^*$, and $|\psi_\infty|^2$ is the velocity, mass, charge, and carrier density respectively. We define $f = \psi/\psi_\infty$ where $\psi_\infty$ is the density deep inside the bulk of the SC, and $\psi_\infty^2 = -\alpha/\beta > 0$ minimizes the free energy deep in the SC bulk (for $\boldsymbol{A} = 0$ and $\nabla\varphi = 0$). Then, if there are no magnetic fields and

$\boldsymbol{A} = 0$, Eq 1.6 becomes (in one dimension):

$$\frac{\hbar^2}{2m^*|\alpha|}\frac{d^2f}{dx^2} + f - f^3 = 0 \tag{1.8}$$

and we can define the GL coherence length:

$$\xi^2_{(GL)} = \frac{\hbar^2}{2m^*|\alpha|}. \tag{1.9}$$

When we use $\frac{1}{2m^*}(\frac{\hbar}{i}\boldsymbol{\nabla} - \frac{e^*}{c}\boldsymbol{A})^2\psi = \frac{m^*v_s^2}{2|\alpha|}\psi$ in Eq 1.6 we obtain:

$$|\psi|^2 = \psi^2_\infty(1 - \frac{m^*v_s^2}{2|\alpha|}) = \psi^2_\infty[1 - (\frac{\xi m^* v_s}{\hbar})^2] \tag{1.10}$$

$$J_s = e^*\psi^2_\infty(1 - \frac{m^*v_s^2}{2|\alpha|})v_s. \tag{1.11}$$

One can see that $J_s$ as a function of $v_s$ reaches a maximum value for a specific velocity. Those are the critical current and the critical velocity:

$$J_c = e^*\psi^2_\infty\frac{2}{3}(\frac{2}{3}\frac{|\alpha|}{m^*})^{1/2}, \tag{1.12}$$

$$v_c = (\frac{2}{3}\frac{|\alpha|}{m^*})^{1/2}. \tag{1.13}$$

so if we measure the critical velocity $v_c$ (or the critial current) we can also find $\xi$ using the relation:

$$\xi = \frac{\hbar}{\sqrt{3}m^*v_c}. \tag{1.14}$$

If we assume that $m^* = 2m_e$ ($m_e$ being the mass of a free electron) and

$e^* = 2e$ ($e$ being the charge of a free electron) we can find from Eq 1.5 that $\beta = |\alpha|\frac{8\pi e^2}{m_e c^2}\lambda^2$, and so $|\psi_\infty|^2 = \frac{m_e c^2}{8\pi e^2 \lambda^2}$. Then, using Eq 1.12, we find:

$$J_c = \frac{m_e c^2}{6\pi e \lambda^2} v_c \tag{1.15}$$

using SI units, we get:

$$J_c^{\mathrm{SI}} = \frac{2m_e}{3\mu_0 e \lambda^2} v_c \tag{1.16}$$

## 1.4 The Cuprates Family

The cuprates are a family of High Temperature SC (HTSC) discovered in 1986 [5]. The cuprates are ceramic, layered materials, containing $CuO_2$ planes separated by non-superconducting layers which act as charge reservoirs. These compounds are anti-ferromagnetic Mott-insulators in the undoped phase, due to strong electron coupling that localizes the electrons. By adding oxygen atoms to the material, electrons are drawn to the oxygen atoms and thus lowering the electron density in each unit cell. The addition of oxygen atoms to the material is called hole doping (the "hole" is the absence of an electron from its position in the atomic lattice). Doping the cuprates with holes weakens the coupling, destroys the long range anti-ferromagnetic order and increases conductivity. Above a certain level of doping, superconductivity emerges. The critical temperature increases with doping up to an optimal doping level. Further doping results in lowering $T_c$ (over-doping) until superconductivity vanishes. In this work we will use the hole-doped

("P type") $Bi_2Sr_2CaCu_2O_{8+x}$ (Bi-2212) cuprate discovered around 1988 [7]; it was the first HTSC with no rare-earth elements, its critical temperature is about $70K$ and its unit cell is presented in Fig 1.2. The phase diagram of these hole-doped cuprates is very rich. Some of the phases seem to be of competing orders, while for others the relation to SC is still under debate. In Fig 1.3 one can see a typical phase diagram of cuprates as a function of doping $p$. In the cuprate superconductors there is a correlation between the superfluid density and the critical temperature, known as the Uemura relation [8], which states that $T_c$ is linearly proportional to the superfluid density as can be seen in Fig 1.1. The superconducting dome ($T_c(p)$) is universal, and using the known relation between p (holes per Cu atom) and $T_c$, we can determine the doping level of our sample using the Tallon-Presland formula [9]:

$$p = 0.16 \pm 0.11003\sqrt{1 - \frac{T_c}{T_c^{max}}}$$

## 1.5 Crystal Making

In this work, the Bi-2212 crystal was grown using a DC sputtering system on a ring shaped STO ($SrTiO_3$) substrate with one side polished and crystallographic plane [100], with an outer diameter of 5mm and an inner diameter of 1mm. Later, the samples were oxidized at 450°C in an oxygen atmosphere. The same sample was re-oxidized following each measurement.

The sputtering system comprises of a vacuum chamber that can be pumped

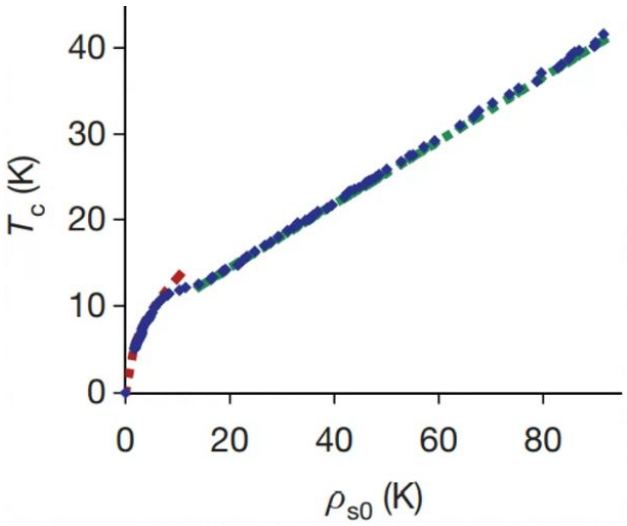


Figure 1.1: The Uemura Relation measured by Božović at al. for LSCO [8]: The dependence of $T_c$ on $\rho_{s0} \equiv \rho_s(T \to 0)$. The experimental data are represented by the blue diamonds; the green dashed line is the fit to $T_c = T_0 + \alpha\rho_{s0}$ with $\alpha = 0.37 \pm 0.02$ for $\rho_{s0} > 15K$ and the red dashed line is the fit to $T_c = \gamma\sqrt{\rho_{s0}}$ with $\gamma = (4.2 \pm 0.5)K^{1/2}$ for $\rho_{s0} < 12K$.

down to around 80 millitorrs of pressure. By injecting oxygen while pumping, the system is able to regulate a constant oxygen atmosphere at a wide range of pressures. Inside the chamber, the STO substrate is held in place by a holder with heating elements that hold the substrate at a determined temperature. A high voltage (up to 500V) is applied between the substrate and the target, which is held a few centimeters below the substrate. The high voltage and the oxygen atmosphere create a plasma environment, as the oxygen ions in the plasma are driven into the target which is held in a negative bias. The bombardment of the ions releases atoms from the target, that condense on the substrate to form a thin film. The target itself

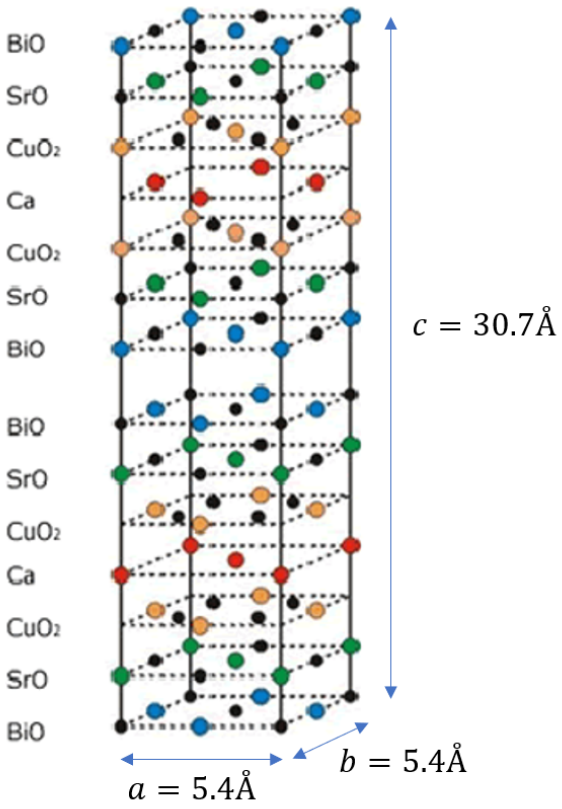


Figure 1.2: Bi-2212 Unit Cell. [10]

comprised of a mixture of $Bi\,Sr\,Ca\,CuO_2$ powder which is repeatedly heated for several hours and mixed again, then compressed into a disk. Optimally, the crystal growth should take place under a 3.5 torr oxygen atmosphere, at 895°C, using 350V between the target and the substrate at a fixed current of 0.12A. These conditions produce a growth rate of about 100 nm/hour, and a overdoped Bi-2212 sample. Then, the oxygen content can be lowerd or raised by heating the sample to 450°C in an oxygen atmosphere at pressures as low as 0.05 torr and up to 400 torrs, using either the sputtering vacuum

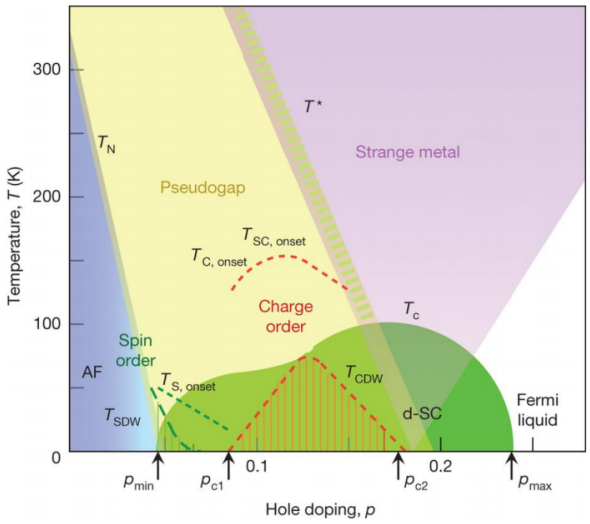


Figure 1.3: Cuprates Phase Diagram: Hole doping $p$ vs. temperature. [11]

chamber for above 1torr of oxygen pressure or the PLD vacuum chamber for lower than 1torr of oxygen pressure. The sputtering system is presented in Fig 1.4.

Figure 1.4: The sputtering system

# 2 Stiffnessometer (Operation Principles)

In this section we will explain the principles of operation of a device developed in our group [1][2], used for measuring stiffness, which is accordingly called a Stiffnessometer. An ideal Stiffnessometer is made of an infinitely long excitation-coil, piercing a ring-shaped sample; when a current $I$ is applied through the coil, one can generate a magnetic field inside this coil without a field outside. With that, there is a vector potential $\boldsymbol{A} = \frac{\mu_0 n I}{r}\hat{\varphi}$ where $n$ is the winding density and $r$ is the distance from the symmetry axis of the coil. If the sample is cooled below $T_c$ without any magnetic field or current in the excitation coil, there will be no vector potential ($\boldsymbol{A} = 0$). We call this cooling process Zero-Gauge-Field-Cooling (ZGFC). When the sample is cooled so that it becomes a SC, it will choose the phase $\varphi$ (in Eq 1.1) such that the free energy is minimized. So, when we follow the ZGFC protocol, the vector potential is zero $\boldsymbol{A} = \boldsymbol{0}$ and so $\nabla\varphi = 0$ and $J = 0$ according to the London equation: Eq 1.2. But now, changing of $\varphi$ is energetically costly for the SC, so when we turn on the current in the coil and $\boldsymbol{A} \neq 0$ we still get $\boldsymbol{J}_s = -\hat{\rho}_s \boldsymbol{A}$, meaning that the vector potential $\boldsymbol{A}$ generates super currents $\boldsymbol{J}_s$ inside the ring. Those super currents are going around in a loop to create a magnetic moment $m$, which can be measured using a pickup-loop connected to a SQUID. The London equation indicates a linear relation between $\boldsymbol{J}_s$ and $\boldsymbol{A}$. Since $\boldsymbol{A}$ is proportional to the current in the excitation coil $I$, and $\boldsymbol{J}_s$ is proportional to the sample's magnetic moment $m$, a linear

relation between the applied current and the measured magnetic moment (see below) is expected. When this linearity breaks, we know that something had changed in the system, meaning that we are above the critical current $I_c$.

There are two types of measurements to choose from: we can stay at a constant temperature while increasing the current $I$; this type of measurement determines the critical vector potential $A^c$, hence $J_c$ and $\xi$. Alternatively, we can change the temperature while the current is in the linear regime and constant; this type of measurement provides the stiffness as a function of temperature.

This new novel technique is used to determine $\rho_s$ and $J_c$ or $\xi$ without a magnetic field. Another advantage of this technique is that it demands a global phase coherence. Therefore, phase transitions are much sharper compared to other techniques such as a transport measurement or the magnetization measurement of the Meissner Effect.

## 2.1 Experimental Setup

The coil we used is 60 mm long with an external diameter of 0.8mm. Comprised of a copper wire of 0.13mm width, it has two layers and 1940 windings in total. The coil goes through the hole of the ring-shaped sample as the ring is at its center. The pickup loop is a static gradiometer with 4 loops, through which the coil and the ring are going up and down. A second external coil is used to cancel external magnetic fields stronger then 0.001 Oe. We used

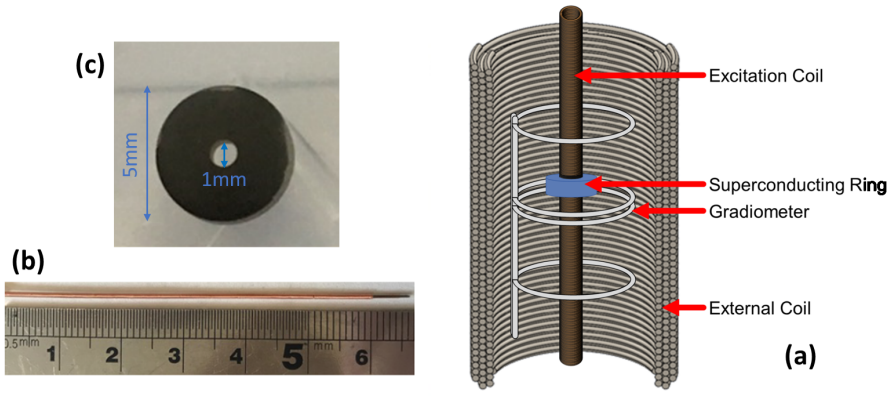


Figure 2.1: (a) Illustration of the long coil with the ring on it, the gradiometer and the external coil. (b) A 60 mm long copper coil. (c) The ring-shaped Bi-2212 sample.

a Quantum Design MPMS3 magnetometer in which the gradiometer is connected to a SQUID measuring the magnetic flux of both the ring and the coil. The SQUID's output voltage is proportional to the magnetic flux through the gradiometer. The output voltage of our device can be translated to units of magnetic moment with a resolution of $1 \cdot 10^{-10} A \cdot m^2$. Because of the gradiometer's geometry the output signal of the SQUID has a unique shape.

## 2.2 SQUID magnetometer

During the measurements, the ring is fixed at the center of the coil and together they move along the $z$ direction (the horizontal axis in Fig. 2.2), in and out of the gradiometer which its center is fixed at $z = 0$. While moving, the magnetic flux through the gradiometer is changing. Figure 2.2 presents

such measurements of a ring above and below $T_c$.

The measurements can be done in two different detection methods:
(I) DC scan mode, in which we record the SQUID's output voltage $V(z)$ while the ring and the excitation coil move relative to the gradiometer. The DC mode allows detection of the excitation coil signal profile as well since the entire coil can be pulled out of the gradiometer. Our gradiometer detects magnetic moments within a range of 40mm on each side of its center. This sets the length of our excitation coil. When measuring over a wide temperature range, detection of the excitation coil's contribution is essential to determine the flux it generates at each temperature.
(II) VSM (Vibrate Sample Magnetometer) mode, where the ring vibrates around the center of the gradiometer with an amplitude of 5mm. Each measurement is averaged over 2 seconds. The motor creates sinusoidal sample motion with a frequency f. Average voltage output is obtained by lock-in detection at a 2f signal. In this mode, the excitation coil does not contribute to the signal significantly. The VSM mode is fast and allows fine temperature scans without needing to achieve temperature stability at each measuring point. Another advantage is that the nulling of the external field is best in a range of 10mm to each side. Hence, the sample remains in the nulled field range during the measurement.

The best way to understand the signal in a measurement of the Stiffnessometer, as illustrated in Fig 2.2, is to look at the raw data of a DC scan. The black squares represent the excitation coil signal moving through

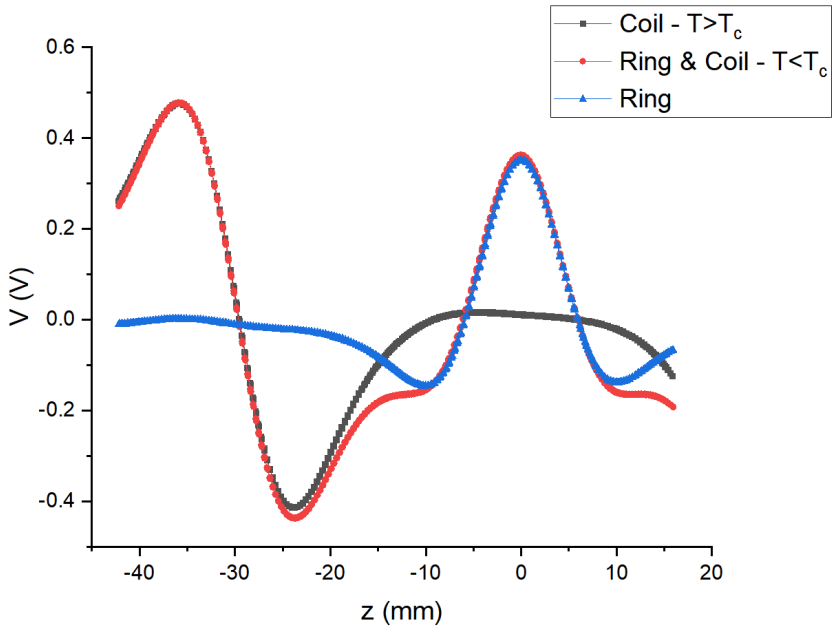


Figure 2.2: A typical DC measurement of a ring in the center of an excitation coil is scanned using a gradiometer connected to a SQUID. At a high-temperature when the ring is not superconducting (in black squares); At a low-temperature when the ring is superconducting (in red circles); and in blue triangles, the difference between these measurements.

the gradiometer at T > Tc. At T < Tc, the ring adds its own signal, as shown by red circles. The ring signal is concentrated on a narrower range on the z axis. By subtracting the high-temperature measurement from the low-temperature one, it is possible to remain with the signal of the ring alone, as demonstrated by the blue triangles.

# 3 Measurements and Results

## 3.1 M(T) Measurement and Results

In this measurement, we cool the system to a base temperature (below $T_c$). Then, we apply a fixed current in the excitation coil. Using the VSM mode, after the system is stabilized, we gradually increase the temperature in a wide range such that we can observe the whole phase transition from the SC phase to the normal phase, as we measure the magnetization.

From each measurement we had subtracted a background signal that was measured with zero current in the excitation coil. In addition, we divided each measurement by the current that was applied for normalization purposes, as it does not affect the stiffness. In Fig. 3.1 we can see the differences between measurements under different currents, caused by the leaking fields that come from the non-ideal (not infinite) coil.

This type of measurement provides our definition of the critical temperature $T_c$: it is the end of the phase transition i.e. the first temperature where the magnetization is zero. In Fig. 3.2 we can see the phase transitions for different doping levels, hence the $T_c$ for each doping.

## 3.2 Critical Current Measurements and Results

For this measurement, we cool the system to a certain temperature below $T_c$ with zero current in the excitation coil. After the temperature has stabilized, we gradually increase the current in the excitation coil while measuring the

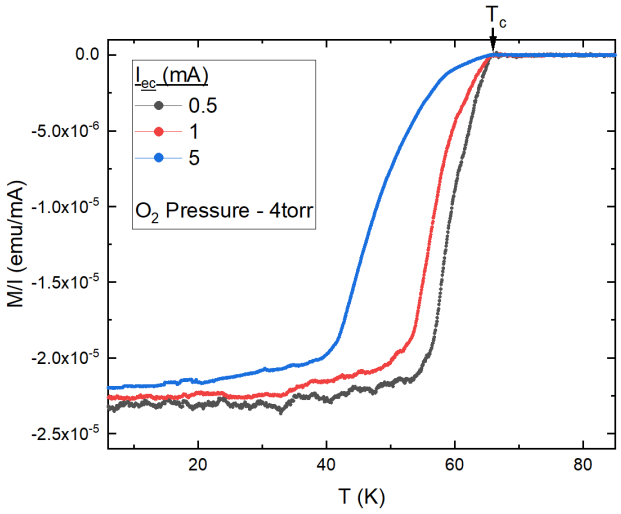


Figure 3.1: M/I measurements as function of the temperature for different currents.

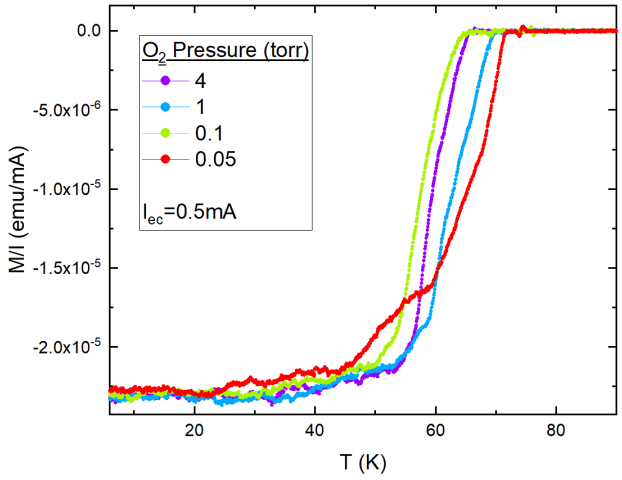


Figure 3.2: M/I measuremenrt as function of the temerature for several samples with different oxygen level for $I_{ec} = 0.5mA$

superconducting magnetic moment, as a practice of the VSM mode. We then subtract the background signal, which is the signal caused by the current at temperatures above $T_c$. This signal is a product of the excitation coil's finite length and asymmetry.

Typical behavior in our measurements, is a linear relation between the magnetic moment of the ring and the current of the excitation coil, at low currents. At some value of current, the linear relation breaks. This value defines the critical current in the ring $I_c$. From that point on, the moment is expected to stop growing with the increasing current and to reach saturation. This measurement is presented in Fig. 3.3 for different temperatures.

We fit each $M(I_{ec})$ in a fixed temperature in the limit of $I_{ec} \to 0$ (before the linearity breaking at $I_c$ ) to a linear line where the slope represents $dM/dI$ as seen in Fig. 3.5 such that we can calculate the penetration depth $\lambda$ from it. The crossing point between the linear line before $I_c$ and the linear line after $I_c$ yields the critical current $I_c$ itself. The results are presented in Fig. 3.4.

The measurements do not cover the entire temperature range up to $T_c$ since defining a linear region before $I_c$ in the $M(I_{ec})$ data becomes difficult as $I_c$ itself goes to zero.

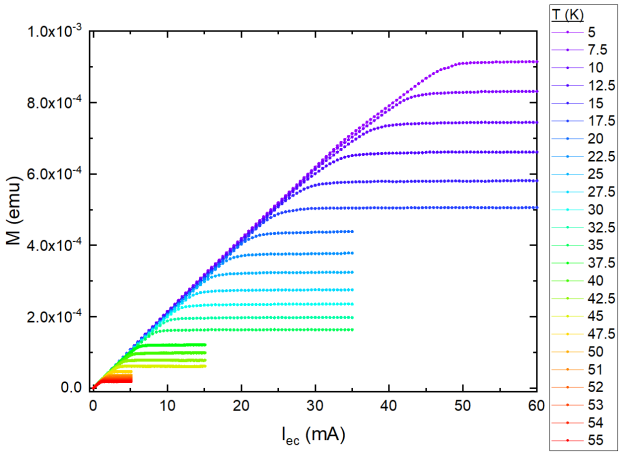


Figure 3.3: Critical current measurements in different temperatures for doping level of 1torr of oxygen pressure

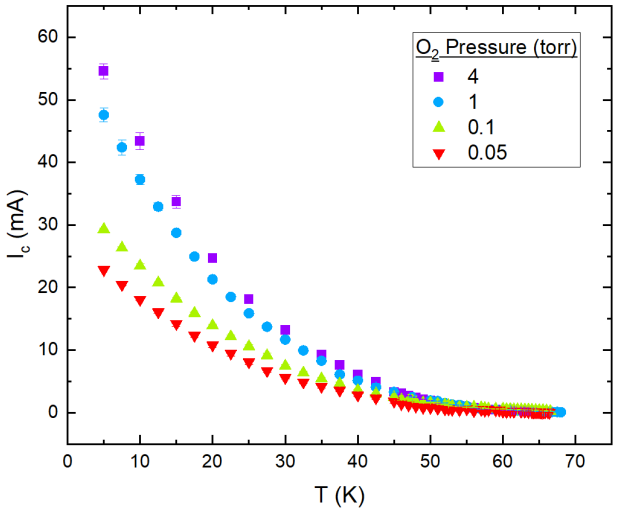


Figure 3.4: Critical currents as function of temperature

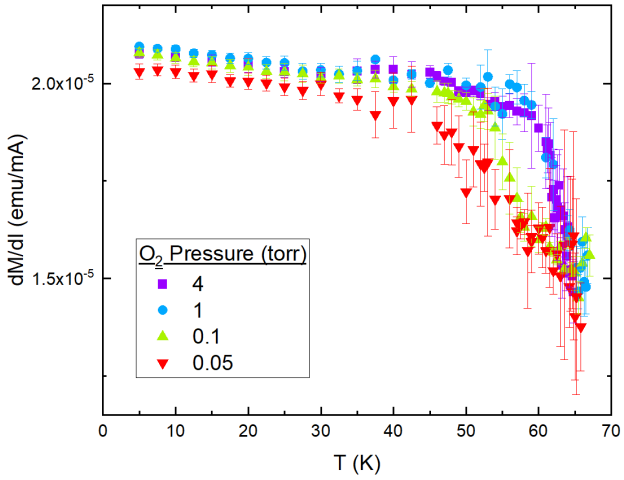


Figure 3.5: dM/dI as function ot temperature

# 4 Data Analysis

## 4.1 Stiffnessometer Theory

Before we find the stiffness or the critical current, we need to deal with the fact that $\boldsymbol{J}_s$ is not equally distributed inside the ring and it might reach its critical value in one place before another. Also, the relevant vector potential in Eq 1.2 $\boldsymbol{A}$ is the total vector potential with a contribution from the vector potential produced by the coil $\boldsymbol{A}_{coil}$ and the vector potential generated by the ring $\boldsymbol{A}_{ring}$. Moreover, our sample is thin with a thicknes of 200nm, a surface super-current density J and a vector potential A that are well defined even for a 2D superconductor. Therefore, the gauge-invariant London equation is given by

$$\boldsymbol{J}_s = \frac{\psi^2}{\mu_0 \Lambda \psi_0^2}\left(\frac{\Phi_0}{2\pi}\boldsymbol{\nabla}\phi - \boldsymbol{A}_{tot}\right) = \frac{\psi^2}{\mu_0 \Lambda \psi_0^2}\left(\frac{\Phi_0}{2\pi}\boldsymbol{\nabla}\phi - \boldsymbol{A}_{coil} - \boldsymbol{A}_{ring}\right)$$

where $\Lambda$ is the Pearl length [12], $\Phi_0$ is the SC flux quanta, and $\psi$ and $\phi$ are the magnitude and phase of the SC order parameter respectively. For a SC of thickness $d \ll \lambda$ , the Pearl length is given by $1/\Lambda = d/\lambda_0^2 = \mu_0 \psi_0^2 e^{*2} d/m^*$ , where $e^*$ and $m^*$ are the carriers' charge and mass respectively, and $\psi_0$ is the equilibrium value of the order parameter in the absence of fields.

By using Maxwell's equation: $\boldsymbol{J} = \frac{1}{\mu_0}\boldsymbol{\nabla} \times \boldsymbol{\nabla} \times \boldsymbol{A} = -\frac{1}{\mu_0}\boldsymbol{\nabla^2 A}$ , we get a

partial differential equation (PDE) for $\boldsymbol{A}_{ring}$:

$$\boldsymbol{\nabla}^2\boldsymbol{A}_{ring} = -\frac{\psi^2}{\Lambda\psi_0^2}\left(\frac{\Phi_0}{2\pi}\boldsymbol{\nabla}\phi - \boldsymbol{A}_{coil} - \boldsymbol{A}_{ring}\right). \tag{4.1}$$

The magnetic flux of the coil through a single pick-up loop is: $\Phi_{coil} = \int \boldsymbol{B}\cdot d\,\boldsymbol{a} = \oint \boldsymbol{A}\cdot d\boldsymbol{l} = \boldsymbol{2\pi}\mu_0 nI$ and we can write 4.1 as: $\boldsymbol{\nabla}^2\boldsymbol{A}_{ring} = \frac{\psi^2}{\Lambda\psi_0^2}(-\frac{\Phi_0}{2\pi}\boldsymbol{\nabla}\phi + \frac{\Phi_{coil}}{2\pi r}\hat{\varphi} + \boldsymbol{A}_{ring})$ where $\hat{\varphi}$ is the azimuthal direction. We switch to unitless parameters by defining:

$$\psi/\psi_0 \to \psi, r/R_{PL} \to r, A_{ring}/A_{coil}(R_{PL}) \to A, \Lambda/R_{PL} \to \Lambda, z/R_{PL} \to z \tag{4.2}$$

where $R_{pl} = 8.5mm$ is the radius of the pick-up loop.

Using cylindrical coordinates and the symmetry of the system ($\boldsymbol{A} = A(r,z)\hat{\varphi}$) we get a unitless PDE:

$$\frac{\partial^2 A}{\partial z^2} + \frac{\partial^2 A}{\partial r^2} + \frac{1}{r}\frac{\partial A}{\partial r} - \frac{A}{r^2} = \frac{\psi^2}{\Lambda}\left(A + \frac{1-m}{r}\right)\delta(z) \tag{4.3}$$

with boundary conditions $A_{sc}(0,z) = A_{sc}(\infty,z) = 0$. In this equation $r$ and $\Lambda$ are measured in units of $R_{pl}$, $\psi(r)$ is normalized to 1 at it's maximum, and the integer $m$ is defined via the relations $\nabla\phi = m\hat{\varphi}/r$. When cooling a superconductor at zero $A$ below $T_c$, $\phi$ is uniform ($m = 0$) in order to minimize the kinetic energy.

The solution was achieved using the $FreeFem++$ software. Fig. 4.1 depicts the numerical solution of the PDE. The Y-axis is the normalized

vector potential $A$ at the ring's height $z = 0$, and the pick-up loop radial location is $r = R_{pl}$. The X-axis is a logarithmic scale of the Pearl length $2\Lambda/R_{pl}$.

Normalizing the vector potential of the SC ring by the vector potential of an infinite coil,

$$A_{sc}\left(R_{pl}\right) = \frac{\mu_0 M}{4\pi R_{pl}^2}\hat{\varphi}$$
$$A_{ec}\left(R_{pl}\right) = \frac{\mu_0 n I}{2R_{pl}}\sum_i r_{ec,i}^2$$

where $M$ is the superconducting magnetic moment, $n$ is the windings per unit length in one layer, $r_{ec,i}$ is the radius of the ith layer, and $I$ is the current of the coil.

We obtain the dimensionless vector potential

$$A\left(z = 0, R_{pl}\right) = \sum_i \frac{g}{2\pi n R_{pl} r_{ec}^2} \cdot \frac{M}{I}$$

where $g$ is a calibration constant. We found $g$ by a comparison to Uemura plot, as seen in Fig. 4.2, as three of the measurements comply with the linearity of the Uemura plot, as expected for the cuprates family.

In Fig. 4.3 we see the penetration depth $\lambda$ calculated for each doping level as function of temperature. $\lambda$ is about $3\mu m$ for the limit where $T$ goes to zero.

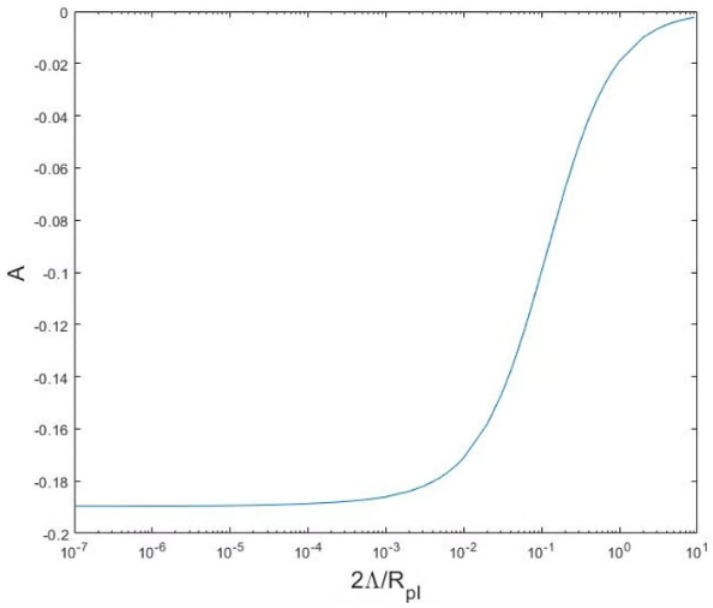


Figure 4.1: Numerical solution of the PDE Eq 4.3 for different $\Lambda$ values, where $R_{pl} = 8.5\,\text{mm}$ is the radius of the pick-up loop. This numerical solution depends on the ring's dimensions.

## 4.2 Coherence length

The current density in the SC is the strongest in the inner radius of the ring [2][13]. Therefore, the destruction of the order parameter starts there and propagates to the outer radius as $J$ increases. We assume that rotation symmetry is respected and no vortices enter the sample, since no external field is applied, and since the magnetization is proportional to the current, even up to $I_c$. Under these assumptions we expect the critical current $I_c$ to show up when $\psi \to 0$ in the entire SC. This allows us to linearize the Ginzburg-Landau equation for $\psi$ and to approximate A by the coil's vector

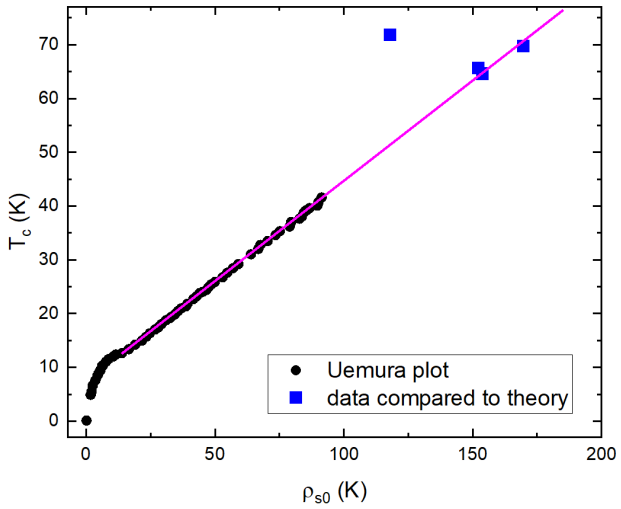


Figure 4.2: Finding the calibration constant g with a comparison to Ueumura plot measured by Božović at al. for LSCO, in black circles [8]. The pink line is the fit to $T_c = T_0 + \alpha\rho_{s0}$ with $\alpha = 0.37 \pm 0.02$ for $\rho_{s0} > 15K$. The blue squers are our measurments after fitting to the pink fit line.

potential. In this case,

$$-\psi_{rr} - \frac{\psi_r}{r} + A_{ec}^2\psi = \frac{1}{\xi^2}\psi$$

The existence of a solution which decays rather than blows-up at small $r$ requires $A_{ec} \leq 1/\xi$. This leads to a critical flux

$$J_c = \frac{\Phi_c}{\Phi_0} \simeq \frac{r_{out}}{\xi}$$

where $\Phi_c = \mu_0 n\pi R_{ec}^2 I_c$, n is the coil's windings density, and $R_{ec}$ is its radius. And then

$$\xi \simeq \frac{2\hbar r_{out}}{\mu_0 n e^* R_{ec}^2 I_c}$$

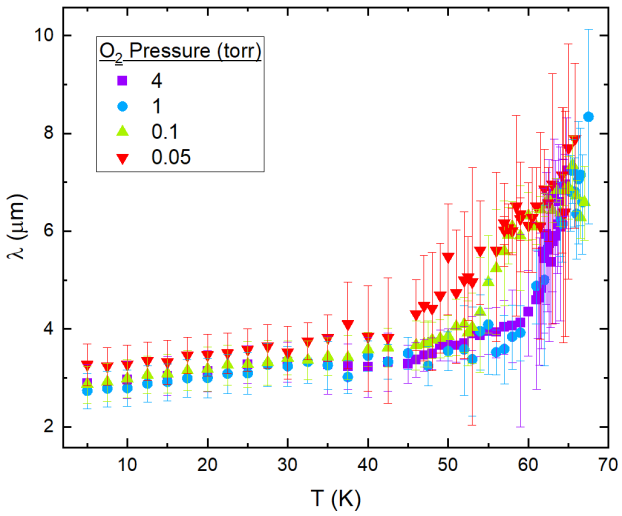


Figure 4.3: The penetration depth as function of temperature for differend doping

Plot of $1/\xi$ as function of the temperature for each doping is presented in Fig. 4.4 , for better view at low temperatures.

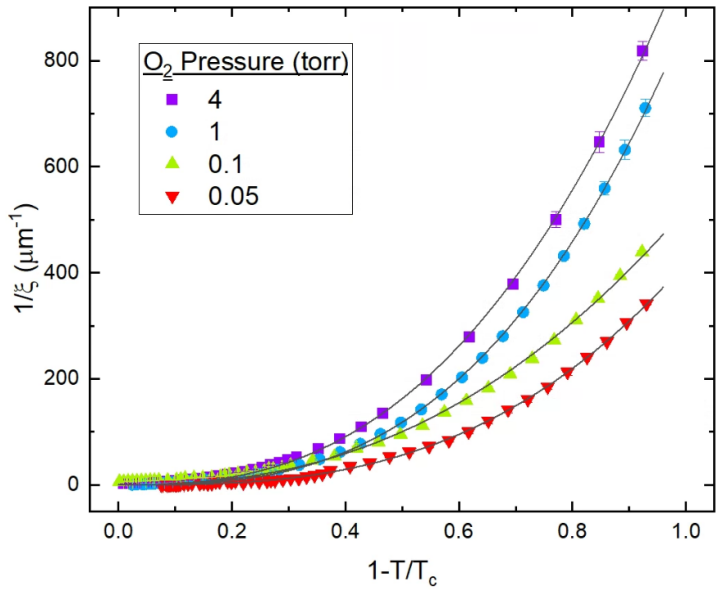


Figure 4.4: Inverted coherence length as function of T for differend doping. The black lines represent fittings to power law.

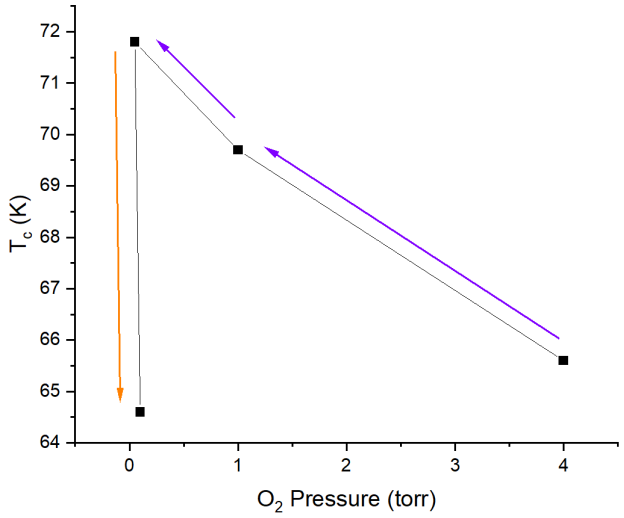


Figure 5.1: $T_c$ as function of $O_2$ pressure. The arrows represent the order of oxidation and measurments. Purple arrows point out oxidations from high pressure to low pressure and orange arrows are for oxidations from low pressure to high pressure.

# 5 Discussion

From Fig. 3.2 we can infer that the dependence of $T_c$ on the doping level is inconsistent. If we commit the sample to oxidize at a low pressure first, and then at a high pressure, we get $T_c$ results that are inconsistent with those produced by oxidation at a high pressure first and then at a low pressure. Hence, it seems more productive to oxidize in only one of the directions in the future.

From Fig. 4.4 we see that $\xi^{-1}$ behaves as power law, therefore we can compare to the GL theory that states

$$\xi^{-1} \propto (1 - T/T_c)^{m_\xi}$$

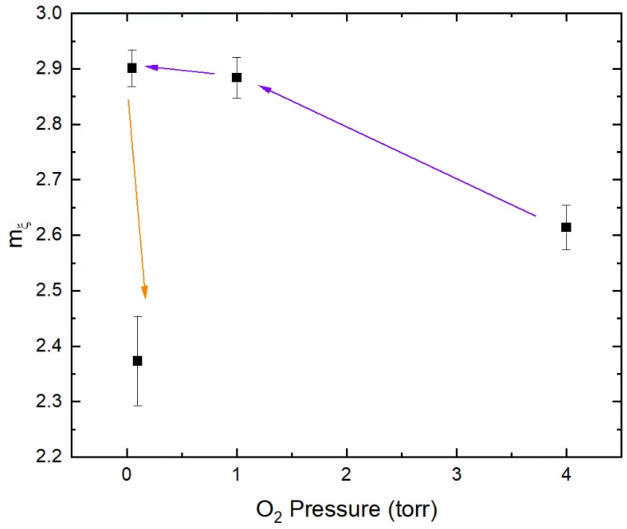


Figure 5.2: $m_\xi$ as function of $O_2$ pressure. The arrows represent the order of oxidation and measurments. Purple arrows point out oxidations from high pressure to low pressure and orange arrows are for oxidations from low pressure to high pressure.

and from fitting the data to a power law we can get the power $m_\xi$ as function of the doping level. We see in Fig. 5.2 a behaviour similar to the dependence of $T_c$ on the doping level: as the concentration of oxygen is consistenetly decrease, the power $m_\xi$ is growing as well. When we change the direction and oxydize from low pressure to high pressure we get inconsistency.

It can be seen in Fig. 5.2 that the yielded $m_\xi$ values are different from the theoretical predicted value of 0.5, though the reason is unclear.

However, we get consistency in the coherence length as a function of the oxidation level, independent of the order of measurments.

At the temperature of 5K we get that the higher the doping level gets, the smaller the coherence length becomes, as presented in Fig. 5.3.

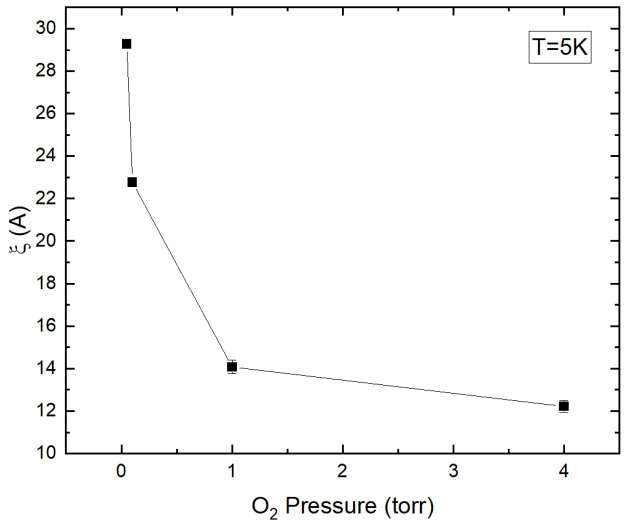


Figure 5.3: $\xi$ as function of $O_2$ pressure at 5K

In a previous work, Wang et al. [14] presents $H_{c2}$ as a function of doping using the vortex-Nernst effect. This was done by measuring the voltage induced by vortex-flow in a driving temperature gradient in a magnetic field. Later, with calculations of the coherence length by $\xi_0 = \sqrt{\Phi_0/2\pi H_{c2}}$ , where $\Phi_0$ is the flux quanta, they concluded that the coherence length is higher for a higher over-doped level, as presented in Fig. 5.4. In addition, these results agree with Pippard length $\xi_p$ obtained from the gap amplitude $\Delta_0$ measured using ARPES [15] by the formula $\xi_p = \hbar v_F/\pi\Delta_0$ where $v_F$ is the Fermi velocity.

Note that we get the same xi values at the range of 12 to 30 angstroms, the equivalence of 3 to 5 lattice parameters. Next, recall that our samples were all within the over-doped regime; the referenced results are included in between the under-doped and the over-doped regimes. Since we can't tell

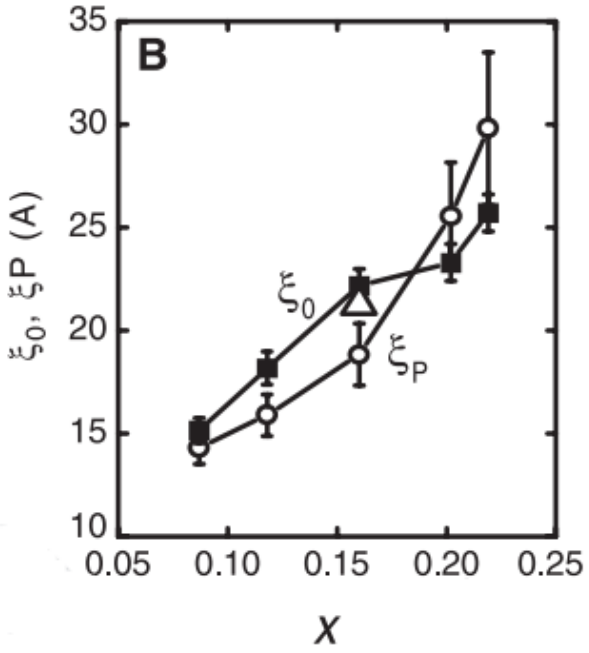


Figure 5.4: Comparison of the coherence length $\xi_0$ (solid squares) obtained from $H_{c2}$ and the Pippard length $\xi_p$ (open circles) obtained from $\Delta_0$ [13]

what is our exact doping level, it might be that our results are a continuation of the older results, meaning that $\xi$ vs. doping curve have a maximum point in that range.

Another difference between our results and Wang's, is that in the paper, the critical field $H_{c2}$ was not measured directly but rather fitted to a known function and was extrapolated in order to achieve $H_{c2}$, the reason for the indirect measurement is the difficulty to produce such high fields of more than 100T. The coherence length results we got were produced by the direct measurement of the critical current.

# 6 Conclusions and Future directions

In this work we measured two SC properties of Bi-2212: the penetration depth and the coherence length. Also, we display the Stiffnessometer measurement technique and explain its methods of operation and data analysis.

Our main findings are:

- We managed to measure the coherence length directly in low temperatures.
- The $T_c$ dependence of doping level is inconsistent for different directions of oxidation order.
- The coherence length is consistently dependent on the oxidation level, regardless of the order of oxidations.
- It was observed that the higher the doping level gets, the smaller the coherence length becomes at low temperatures.

For future inquiries:

- It is preferable to oxidize in only one of the directions: from low to high oxidation level or from high to low only.
- Preparation of thinner samples (under 200nm) is desirable, for better agreement with the coherence length calculation assumptions such that we will get $h \ll \lambda$ .

- In order to collect more comprehensive results, it is recommended to oxidize under smaller pressuers of oxygen to achieve an under-doped regime.

# Bibliography

[**1**] Mangel, I., Kapon, I., Blau, N., Golubkov, K., Gavish, N., & Keren, A. (2020). Stiffnessometer: A magnetic-field-free superconducting stiffness meter and its application. Physical Review B, 102(2), 024502.

[**2**] Keren, A., Blau, N., Gavish, N., Kenneth, O., Ivry, Y., & Suleiman, M. (2022). Stiffness and coherence length measurements of ultra-thin superconductors, and implications for layered superconductors. Superconductor Science and Technology.

[**3**] Bardeen, J., Cooper, L. N., & Schrieffer, J. R. (1957). Microscopic theory of superconductivity. Physical Review, 106(1), 162.

[**4**] Bardeen, J., Cooper, L. N., & Schrieffer, J. R. (1957). Theory of superconductivity. Physical review, 108(5), 1175.

[**5**] Bednorz, J. G., & Müller, K. A. (1986). Possible highT c superconductivity in the Ba− La− Cu− O system. Zeitschrift für Physik B Condensed Matter, 64(2), 189-193.

[**6**] Tinkham, M. (2004). Introduction to superconductivity. Courier Corporation.

[**7**] Maeda, H., Tanaka, Y., Fukutomi, M., & Asano, T. (1988). A new high-Tc oxide superconductor without a rare earth element. Japanese Journal of Applied Physics, 27(2A), L209.

[**8**] Božović, I., He, X., Wu, J., & Bollinger, A. T. (2016). Dependence of the critical temperature in overdoped copper oxides on superfluid density. Nature, 536(7616), 309-311.

[**9**] Presland, M. R., Tallon, J. L., Buckley, R. G., Liu, R. S., & Flower, N. E. (1991). General trends in oxygen stoichiometry effects on Tc in Bi and Tl superconductors. Physica C: Superconductivity, 176(1-3), 95-105.

[**10**] Vastola, J. (2016). The Effect of Impurities on the Superconductivity of BSCCO-2212.

[**11**] Keimer, B., Kivelson, S. A., Norman, M. R., Uchida, S., & Zaanen, J. (2015). From quantum matter to high-temperature superconductivity in copper oxides. Nature, 518(7538), 179-186.

[**12**] Pearl, J. (1964). Current distribution in superconducting films carrying quantized fluxoids. Applied Physics Letters, 5(4), 65-66.

[**13**] Gavish, N., Kenneth, O., & Keren, A. (2021). Ginzburg–Landau model of a Stiffnessometer—A superconducting stiffness meter device. Physica D: Nonlinear Phenomena, 415, 132767.

[**14**] Wang, Y., Ono, S., Onose, Y., Gu, G., Ando, Y., Tokura, Y., ... & Ong, N. P. (2003). Dependence of upper critical field and pairing strength on doping in cuprates. Science, 299(5603), 86-89.

[**15**] Ding, H., Engelbrecht, J. R., Wang, Z., Campuzano, J. C., Wang, S. C., Yang, H. B., ... & Hinks, D. G. (2001). Coherent quasiparticle weight

and its connection to high-T c superconductivity from angle-resolved photoemission. Physical review letters, 87(22), 227001.

של שדה מגנטי בדגם; באופן זה אנו נמנעים מסיבוכים של גורם דימגנטיזציה ומקיומן של מערבולות זרם (Vortices).

בשנת 1986 התגלו חומרים מוליכי על בטמפרטורות גבוהות שהם מבוססי נחושת (משפחת הקופרטים). הקופרטים הם תרכובות קרמיות העשויות שכבות ביניהן שכבות של תחמוצת הנחושת $CuO_2$. תרכובות אלו בבסיסן הן מבודדים אנטי־פרומגנטיים, הודות לאינטראקציות חזקות בין האלקטרונים. על ידי אילוח (סימום) חומרים אלה, ניתן להגדיל את מספר האלקטרונים או החורים החופשיים בחומר ולגרום להעלמות הפאזה האנטי־פרומגנטית ולהופעה של הפאזה העל מוליכה. בעבודה זו, ביצענו מחקר על דגם Bi-2212 ($Bi_2Sr_2CaCu_2O_{8+x}$). על־מוליך זה ניתן לסימום חורים על ידי הוספה של אטומי חמצן. תחילה, הטמפרטורה הקריטית עולה עם הוספת החורים עד להגעה לטמפרטורה קריטית מקסימלית עם ערך של 0.16 חורים לתא יחידה; ערך זה נקרא סימום אופטימלי. הוספה של חורים מעבר לכך תגרום לירידה של הטמפרטורה הקריטית עד להעלמות הפאזה העל מוליכה. בנוסף, הקופרטים מקיימים קשר לינארי בין קשיחות העל מוליכות ובין הטמפרטורה הקריטית הנקרא קשר יומורה (The Uemura Relation).

בעבודה זו גידלנו דגם של על־מוליך Bi-2212 בעל טמפרטורה קריטית של כ־$70K$ באמצעות מערכת מסוג DC - sputtering. לאחר כל מדידה, הדגם סומם בתחום סימום־היתר על ידי חימום לטמפרטורה של 450 מעלות צלזיוס באטמוספרה של חמצן בלחצים שונים. בנוסף, מדדנו את קשיחות העל־מוליכות ואת אורך הקוהרנטיות בטמפרטורות שונות ובסימומים שונים. התוצאות מציגות את התלות של הקשיחות ואורך הקוהרנטיות ברמת הסימום. לבסוף, הצלחנו להראות שניתן למדוד את אורך הקוהרנטיות של קופרטים בטמפטורות נמוכות בצורה פשוטה וקלה ליישום שלא דורשת שדות מגנטיים גבוהים בצורה מדוייקת. בדומה לתוצאות של מחקרים קודמים, התקבל אורך קוהרנטיות המקביל בגודלו לגודל של מספר תאי יחידה.

# תקציר

קשיחות העל־מוליכות $\hat{\rho}_s$ מביעה את היחס שבין הפוטנציאל הוקטורי המגנטי $\boldsymbol{A}$ וצפיפות זרם העל־מוליכות $\boldsymbol{J}_s$ בתוך מוליך־על לפי משוואת לונדון $\boldsymbol{J}_s = \hat{\rho}_s \boldsymbol{A}$. אורך הקוהרנטיות הוא השני מבין שני פרמטרי האורך של העל־מוליכות בתורה של גינזבורג ולנדאו. גודל זה מאפיין את המרחק הקצר ביותר בו פרמטר הסדר $\Psi(r)$ יכול להשתנות מבלי לגרום לעלייה מיותרת באנרגיה.

בדרך כלל, קשיחות העל־מוליכות ואורך הקוהרנטיות נמדדים על ידי הפעלת שדות מגנטיים חיצוניים ומדידת עומק החדירה שלהם לתוך החומר $\lambda$ והשדה הקריטי השני $H_{c2}$. עבור מוליכי על מבוססי נחושת (הקופרטים) מדידות אלה דורשות הפעלת שדה מגנטי גבוה מ־ $100T$, שדה גבוה שקשה מאוד ליצור.

לעומת זאת, אנו מודדים את קשיחות העל־מוליכות ואת אורך הקוהרנטיות באמצעות שיטה שפותחה בקבוצת המחקר שלנו ונקראת `קשיחומטר` (Stiff-nessometer). המדידה מתבצעת על־ידי הזרמת זרם חשמלי דרך סליל־עירור דק וארוך העובר דרך דגם על־מוליך בצורת טבעת. הזרמת זרם בסליל העירור יוצרת שדה מגנטי בחלקו הפנימי של הסליל בלבד כך שהשדה מחוץ לסליל נשאר אפס ולמרות זאת בתוך הטבעת העל מוליכה מושרה פוטנציאל וקטורי מגנטי חסר רוטור $\boldsymbol{A}$. לפי משוואת לונדון מתעוררים בטבעת זרמי התמד על־מוליכים $\boldsymbol{J}_s$ אשר מקיפים את הטבעת ויוצרים מומנט מגנטי אותו ניתן למדוד באמצעות מגנטומטר SQUID (מכשיר התאבכות קוונטית מוליך־על). מכיוון שעוצמת הזרם בסליל העירור ידועה לנו, ניתן לחשב את וקטור הפוטנציאל המופעל ולחשב את הקשיחות מתוך משוואת לונדון. על ידי הגברת הזרם שעובר בסליל העירור ניתן להגדיל ברציפות את הפוטנציאל הוקטורי המגנטי עד שהקשר הלינארי בין $\boldsymbol{J}_s$ ל־ $\boldsymbol{A}$ נשבר. מתוך פתרון של משוואות גינזבורג־לנדאו בתחומים המתאימים ניתן לקשר את צפיפות הזרם הקריטית לאורך הקוהרנטית. שיטה זו מדויקת במיוחד בקרבת הטמפרטורה הקריטית והיא מאפשרת לחקור על־מוליכים ללא שימוש במגעים או נוכחות

מחברת חיבור זה מצהירה כי המחקר, כולל איסוף הנתונים, עיבודם והצגתם, התייחסות והשוואה למחקרים קודמים וכו', נעשה כולו בצורה ישרה, כמצופה ממחקר מדעי המבוצע לפי אמות המידה האתיות של העולם האקדמי. כמו כן, הדיווח על המחקר ותוצאותיו בחיבור זה נעשה בצורה ישרה ומלאה, לפי אותן אמות מידה.

המחקר נעשה בהנחיית פרופסור עמית קרן בפקולטה לפיזיקה

אני מודה לטכניון על התמיכה הכספית הנדיבה בהשתלמותי

# תלות אורך הקוהרנטיות ברמת הסימום עבור קופרטים

**חיבור על מחקר**

**לשם מילוי חלקי של הדרישות לקבלת התואר מגיסטר**

**למדעים בפיסיקה**

**שיר דובנקו**

**הוגש לסנט הטכניון - מכון טכנולוגי לישראל**

אדר, התשפ"ג, חיפה, מרץ, 2023

# תלות אורך הקוהרנטיות ברמת הסימום עבור קופרטים

שיר דובנקו